European Journal of Organic Chemistry

Supporting Information

Neighboring Group Participation of Benzoyl Protecting Groups in C3- and C6-Fluorinated Glucose

Kim Greis, Carla Kirschbaum, Giulio Fittolani, Eike Mucha, Rayoon Chang, Gert von Helden, Gerard Meijer, Martina Delbianco, Peter H. Seeberger, and Kevin Pagel*

Contents

Experimental Details

Mass Spectrometry and Infrared Spectroscopy

Infrared (IR) and mass spectra (Figures 1-2 and S2-S6) of glycosyl cations formed by in-source fragmentation of precursor ions were obtained using a custom setup that combines mass spectrometry with IR spectroscopy in helium droplets (Figure S1). The instrument is described in the following paragraphs. The precursor building blocks were dissolved in a 9:1 (V:V) mixture of acetonitrile and deionized water to yield 0.1 mM solutions. The solutions were ionized *via* nanoelectrospray ionization (nESI) using Pd/Pt coated glass capillaries (Sputter Coater HR 208, *Cressington*), pulled to a tip with an inner diameter of 1-2 μm with a micropipette puller (Model P-1000, *Sutter Instrument*). Bare glycosyl cations are generated by applying a voltage of 1 kV to the tip of the capillary using a Z-spray source.

The generated beam of ions traverses two ring-electrode ion guides and a quadrupole mass filter that allows mass-to-charge selection of the ions of interest. Mass-selected ions are then guided into a hexapole ion trap by a quadrupole bender. The trapped ions are thermalized by collisions with helium buffer gas. The ion trap is cooled to ca. 90 K by liquid nitrogen.

Superfluid helium droplets, generated by a pulsed Even-Lavie valve, traverse the ion trap to pick up ions and rapidly cool them to 0.4 K. They guide the embedded ions to a detection region, where vibrational modes of the embedded ions are excited by an IR beam of the Fritz Haber Institute free-electron laser (FHI FEL[1]). Absorption of multiple resonant photons eventually leads to the release of the ions from the helium droplet and subsequent detection by a time-of-flight detector. Plotting the ion signal as a function of the IR wavenumber yields an IR spectrum. The observed intensities scale non-linearly with the energy of the IR beam because of the multiphoton absorption process. A first-order correction is performed by dividing the ion signal by the energy of the IR macropulse.

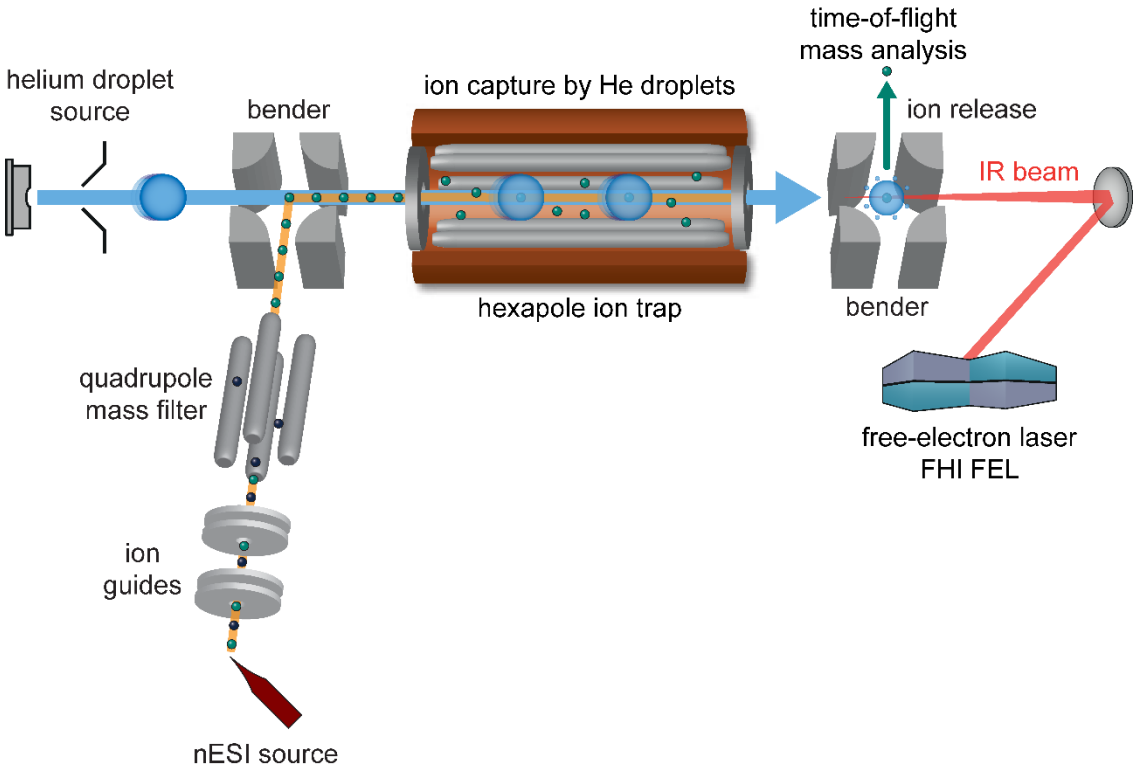

Figure S1. Schematic representation of the helium droplet instrument that combines mass spectrometry with infrared spectroscopy used to generate glycosyl cations and probe their vibrational modes.

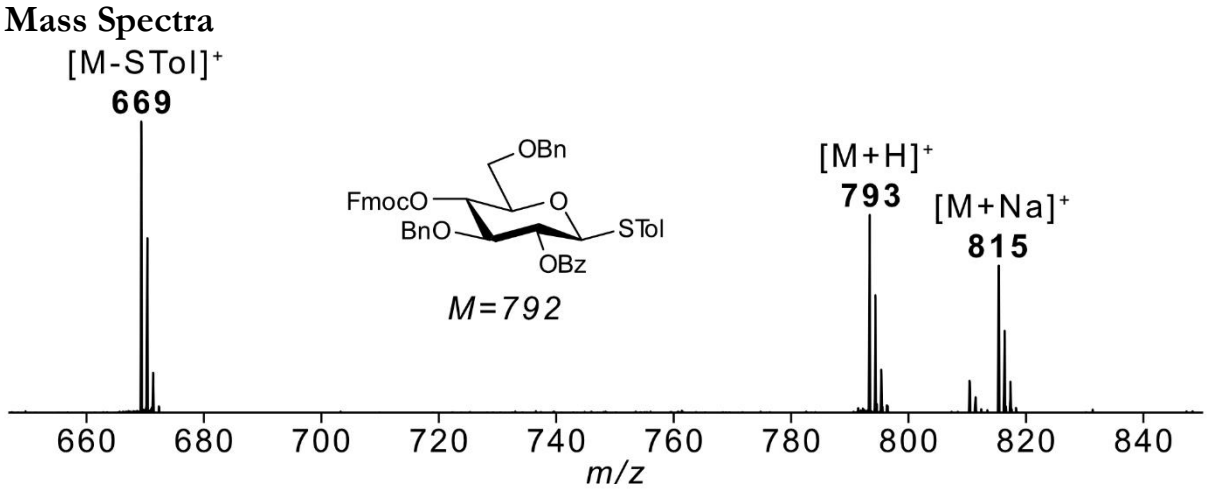

Figure S2. Mass spectrum of 2-*O*-benzoyl-3,6-di-*O*-benzyl-4-*O*-fluorenylmethoxycarbonyl-D-glucopyranoside (**Glc1**) generated from β-thiotolyl precursor recorded on the helium droplet instrument. In-source fragmentation of the precursor ions $[M+H]^+$ (*m/z* = 793), $[M+NH_4]^+$ (*m/z* = 810) and $[M+Na]^+$ (*m/z* = 815) leads to glycosyl cations (*m/z* = 669).

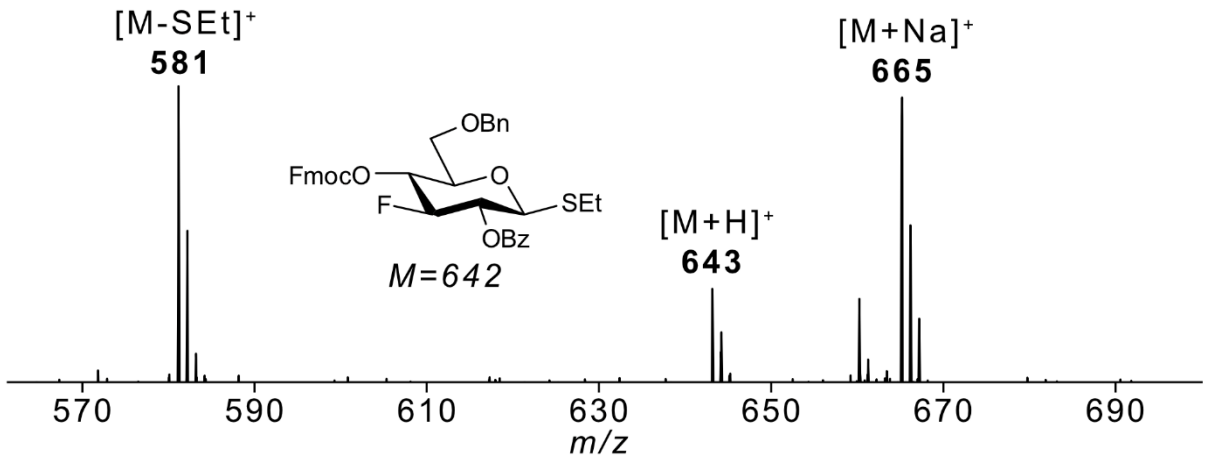

Figure S3. Mass spectrum of 2-*O*-benzoyl-3-F-4-*O*-fluorenylmethoxycarbonyl-6-*O*-benzyl-D-glucopyranoside (**3F-Glc1**) generated from β-thioethyl precursor recorded on the helium droplet instrument. In-source fragmentation of the precursor ions $[M+H]^+$ (*m/z* = 643), $[M+NH_4]^+$ (*m/z* = 660) and $[M+Na]^+$ (*m/z* = 665) leads to glycosyl cations (*m/z* = 581).

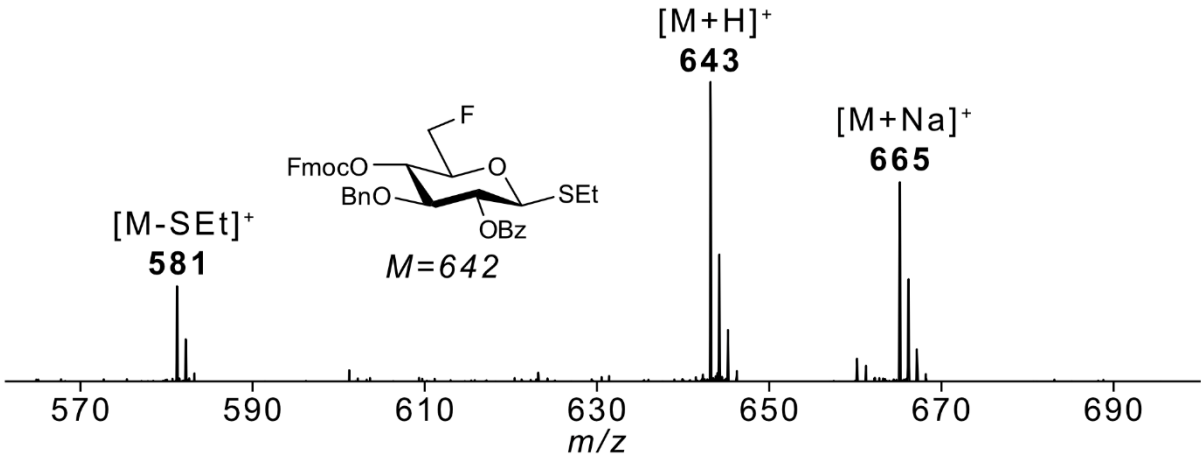

Figure S4. Mass spectrum of 2-*O*-benzoyl-3-*O*-benzyl-4-*O*-fluorenylmethoxycarbonyl-6-F-D-glucopyranoside (**6F-Glc1**) generated from β-thioethyl precursor recorded on the helium droplet instrument. In-source fragmentation of the precursor ions $[M+H]^+$ (*m/z* = 643), $[M+NH_4]^+$ (*m/z* = 660) and $[M+Na]^+$ (*m/z* = 665) leads to glycosyl cations (*m/z* = 581).

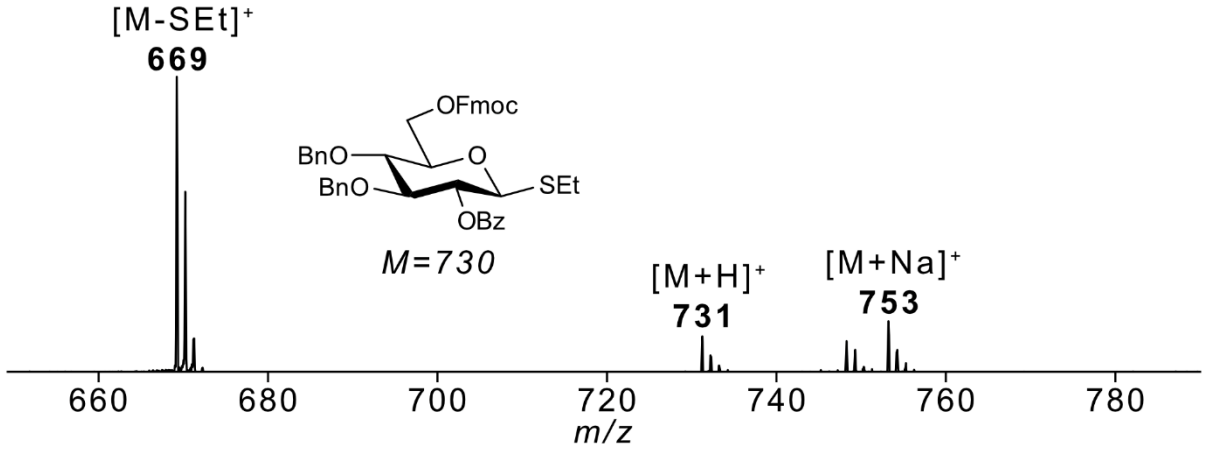

Figure S5. Mass spectrum of 2-*O*-benzoyl-3,4-di-*O*-benzyl-6-*O*-fluorenylmethoxycarbonyl-D-glucopyranoside (**Glc2**) generated from β-thioethyl precursor recorded on the helium droplet instrument. In-source fragmentation of the precursor ions $[M+H]^+$ (*m/z* = 731), $[M+NH_4]^+$ (*m/z* = 748) and $[M+Na]^+$ (*m/z* = 753) leads to glycosyl cations (*m/z* = 669).

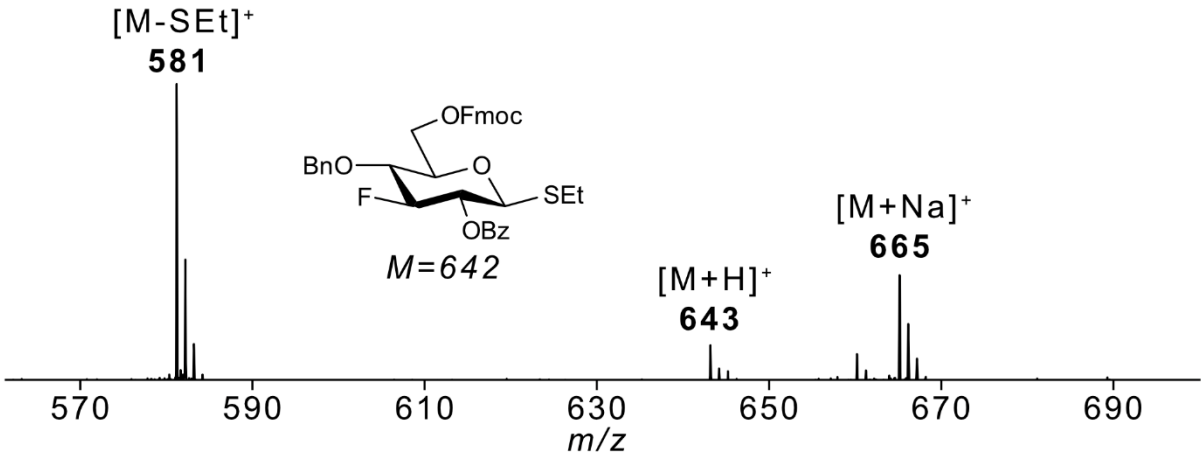

Figure S6. Mass spectrum of 2-*O*-benzoyl-3-F-4-*O*-benzyl-6-*O*-fluorenylmethoxycarbonyl-D-glucopyranoside (**3F-Glc2**) generated from β-thioethyl precursor recorded on the helium droplet instrument. In-source fragmentation of the precursor ions $[M+H]^+$ (*m/z* = 643), $[M+NH_4]^+$ (*m/z* = 660) and $[M+Na]^+$ (*m/z* = 665) leads to glycosyl cations (*m/z* = 581).

Computational Methods

The conformational space of fluorinated glycosyl cations and that of their non-fluorinated counterparts was sampled using the genetic algorithm (GA) FAFOOM.[2] It allows sampling of all rotatable bonds and pyranose puckers. In this study, an interface of the GA with ORCA 4.1.1[3] was used for geometry optimization of each generated structure at the PBE/def2-SVP[4] level of theory. For each glycosyl cation, ten individual GA runs with the settings specified in Table S1 were carried out. The total number of generated structures can be found in Table S2 and their energy hierarchies in Figure S7. The GA yielded structures with four distinct modes of participation (Scheme 1): (**I**) dioxolenium-type structures exhibiting neighboring group participation of the C2-benzoyl protecting group, (**II**) dioxolenium-type structures exhibiting remote participation of the C4- (or C6-)Fmoc protecting group, (**III**) oxonium-type structures exhibiting *non-classical* remote participation of a C6-benzyl protecting group (only visible for **Glc1** and **3F-Glc1** glycosyl cations), and (**IV**) oxocarbenium-type structures exhibiting no participation (3D structures in Figures S9-S13).

Table S1. GA parameters used in initial search.

	Parameter	Value
Molecule	Distance_cutoff_1	1.2
	Distance_cutoff_2	2.15
	Rmsd_cutoff_uniq	0.25
GA settings	Popsize	10
	Prob_for_crossing	0.95
	Prob_for_mut_pyranosering	0.6
	Prob_for_mut_torsion	0.8
	Fitness_sum_limit	1.2
	Selection	Roulette wheel
	Max_mutations_torsion	3
	Max_mutations_pyranosering	1

For each mode of participation a certain number of low-energy structures, specified in Table S2, were reoptimized and frequencies computed at the PBE0+D3/6-311+G(d,p)[5] level of theory with default settings using Gaussian 16, Revision A.03.[6] Energies including zero-point vibrational energies and free energies at 90 K (according to experimental conditions in the hexapole ion trap) of the reoptimized geometries can be found in Tables S3–S7. Free energy hierarchies are shown in Figure S8. It is clearly distinguishable that structures exhibiting neighboring group participation of C2-benzoyl protecting groups are the most favored structural motif. All computed IR spectra were normalized and scaled by a factor of 0.965 (Figures 1 and 2).

Table S2. Number of generated structures for during GA and reoptimized structures. (**I**) neighboring group, (**II**) remote participation, (**III**) *non-classical* remote participation, and (**IV**) no participation.

Glycosyl Cations	#(GA Structures)	#(Reoptimized Structures)			
		I	**II**	**III**	**IV**
Glc1	214	10	5	5	5
3F-Glc1	314	10	5	5	5
6F-Glc1	316	10	5	/	5
Glc2	245	10	3	/	5
3F-Glc2	310	10	5	/	5

Energetics

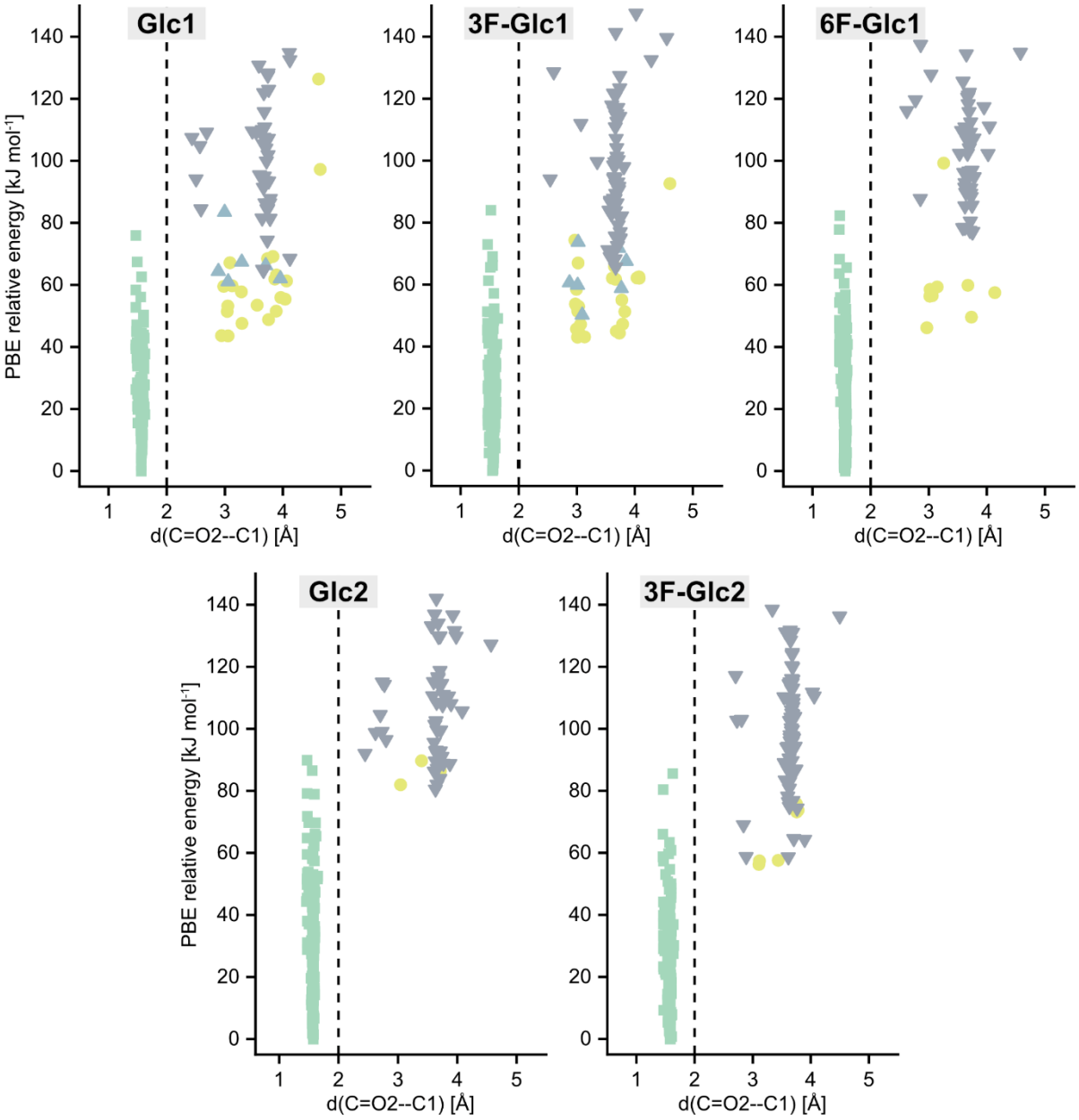

Figure S7. Energy hierarchies of sampled **Glc1**, **3F-Glc1**, **6F-Glc1**, **Glc2**, and **3F-Glc2** glycosyl cations as a function of the distance between the carbonyl oxygen of the C2-benzoyl protecting group and the anomeric carbon (C1). Energies were computed based on optimized geometries at the PBE/def2-SVP level of theory. Green squares indicate structures exhibiting C2-benzoyl neighboring group participation (**I**, dioxolenium), yellow circles C4-Fmoc remote participation (**II**, dioxolenium), blue triangles *non-classical* C6-benzyl remote participation (**III**, oxonium, only possible for **Glc1** and **3F-Glc1**), and gray triangles no participation (**IV**, oxocarbenium).

Table S3. List of reoptimized geometries of the **Glc1** glycosyl cation at the PBE0+D3/6-311+G(d,p) level of theory. Ring puckers, bond distances between the carbonyl oxygen of the C2-benzoyl group and the anomeric carbon (C1), energies (Δ*E*, including zero-point-vibrational energy) and free energies (Δ*F*) at 90 K are assigned to each structure. The infrared spectra of the structures labelled with a roman number are represented in the manuscript.

ID	Ring Pucker	d(C2=O—C1) [Å]	Δ*E*(PBE0+D3) [kJ mol^{-1}]	Δ*F*(PBE0+D3) [kJ mol^{-1}]
C2_Bz_NGP/conf_00 (**I**)	O,3B	1.51	0.00	0.00
C2_Bz_NGP/conf_01	3S1	1.51	3.45	3.38
C2_Bz_NGP/conf_02	O,3B	1.52	7.73	8.34
C2_Bz_NGP/conf_03	3S1	1.51	9.19	7.06
C2_Bz_NGP/conf_04	3S1	1.52	23.94	21.91
C2_Bz_NGP/conf_05	3S1	1.52	19.02	17.66
C2_Bz_NGP/conf_06	3S1	1.52	16.20	14.92
C2_Bz_NGP/conf_07	OS2	1.53	23.04	21.71
C2_Bz_NGP/conf_08	O,3B	1.52	34.56	31.66
C2_Bz_NGP/conf_09	OH5	1.51	18.81	19.05
C4_Fmoc_RP/conf_00	5S1	3.04	61.49	61.49
C4_Fmoc_RP/conf_01	B1,4	3.24	61.90	61.84
C4_Fmoc_RP/conf_02	5S1	3.61	76.87	74.13
C4_Fmoc_RP/conf_03 (**II**)	5S1	2.99	59.86	59.44
C4_Fmoc_RP/conf_04	5S1	3.00	87.16	82.03
C6_OBn_RP/conf_00	EO	2.95	58.52	57.63
C6_OBn_RP/conf_01 (**III**)	1C4	4.00	58.72	57.28
C6_OBn_RP/conf_02	BO,3	2.88	81.01	80.14
C6_OBn_RP/conf_03	BO,3	3.76	75.97	72.94
C6_OBn_RP/conf_04	1C4	2.99	65.68	64.89
oxocarbenium/conf_00 (**IV**)	2SO	3.72	83.38	80.03
oxocarbenium/conf_01	2H3	3.76	94.40	91.63
oxocarbenium/conf_02[(a)]	5S1	3.77	83.99	81.17
oxocarbenium/conf_03	5H4	3.54	116.06	108.67
oxocarbenium/conf_04	2H3	3.74	112.00	108.98

(a) The structure "oxocarbenium/conf_02" converged into a dioxolenium-type structure exhibiting remote participation of the C4-Fmoc protecting group after reoptimization of the geometry at the PBE0+D3/6-311+G(d,p) level of theory and was therefore not further considered.

Table S4. List of reoptimized geometries of the **3F-Glc1** glycosyl cation at the PBE0+D3/6-311+G(d,p) level of theory. Ring puckers, bond distances between the carbonyl oxygen of the C2-benzoyl group and the anomeric carbon (C1), energies (Δ*E*, including zero-point-vibrational energy) and free energies (Δ*F*) at 90 K are assigned to each structure. The infrared spectra of the structures labelled with a roman number are represented in the manuscript.

ID	Ring Pucker	d(C2=O—C1) [Å]	Δ*E*(PBE0+D3) [kJ mol^{-1}]	Δ*F*(PBE0+D3) [kJ mol^{-1}]
C2_Bz_NGP/conf_00 (**I**)	3S1	1.50	0.00	0.00
C2_Bz_NGP/conf_01	3S1	1.50	0.00	0.00
C2_Bz_NGP/conf_02	3S1	1.51	8.31	6.09
C2_Bz_NGP/conf_03	3S1	1.51	4.86	4.23
C2_Bz_NGP/conf_04	O,3B	1.50	11.31	9.09
C2_Bz_NGP/conf_05	5E	1.46	20.59	19.95
C2_Bz_NGP/conf_06	3S1	1.51	7.12	6.75
C2_Bz_NGP/conf_07	5H4	1.49	29.67	26.37
C2_Bz_NGP/conf_08	3S1	1.51	7.13	6.76
C2_Bz_NGP/conf_09	OH5	1.50	13.49	12.72
C4_Fmoc_RP/conf_00	5S1	2.98	72.22	68.65
C4_Fmoc_RP/conf_01	B1,4	4.08	57.06	55.23
C4_Fmoc_RP/conf_02	3S1	2.92	56.48	55.94
C4_Fmoc_RP/conf_03 (**II**)	5S1	4.11	54.64	54.54
C4_Fmoc_RP/conf_04	3S1	2.92	81.18	76.80
C6_OBn_RP/conf_00 (**III**)	1C4	2.92	54.41	51.67
C6_OBn_RP/conf_01	1C4	3.71	69.85	67.04
C6_OBn_RP/conf_02	1C4	3.03	72.97	69.27
C6_OBn_RP/conf_03	BO,3	2.84	83.01	77.84
C6_OBn_RP/conf_04	1C4	4.02	67.80	65.57
oxocarbenium/conf_00 (**IV**)	2SO	3.68	75.16	71.78
oxocarbenium/conf_01	5H4	3.56	80.98	76.03
oxocarbenium/conf_02	5H4	3.54	90.06	85.90
oxocarbenium/conf_03[(a)]	1C4	3.99	66.71	65.13
oxocarbenium/conf_04	3H4	3.33	93.88	90.99

(a) The structure "oxocarbenium/conf_03" converged into an oxonium-type structure exhibiting *non-classical* remote participation of a C6-benzyl group after reoptimization of the geometry at the PBE0+D3/6-311+G(d,p) level of theory and was therefore not further considered.

Table S5. List of reoptimized geometries of the **6F-Glc1** glycosyl cation at the PBE0+D3/6-311+G(d,p) level of theory. Ring puckers, bond distances between the carbonyl oxygen of the C2-benzoyl group and the anomeric carbon (C1), energies (Δ*E*, including zero-point-vibrational energy) and free energies (Δ*F*) at 90 K are assigned to each structure. The infrared spectra of the structures labelled with a roman number are represented in the manuscript.

ID	Ring Pucker	d(C2=O—C1) [Å]	Δ*E*(PBE0+D3) [kJ mol^{-1}]	Δ*F*(PBE0+D3) [kJ mol^{-1}]
C2_Bz_NGP/conf_00	3S1	1.52	2.14	2.00
C2_Bz_NGP/conf_01 (**IA**)	3S1	1.51	0.00	0.00
C2_Bz_NGP/conf_02	3S1	1.50	0.76	0.59
C2_Bz_NGP/conf_03	3S1	1.50	2.22	2.41
C2_Bz_NGP/conf_04	3S1	1.52	5.14	4.24
C2_Bz_NGP/conf_05	3S1	1.53	0.97	2.88
C2_Bz_NGP/conf_06	3S1	1.52	5.14	4.28
C2_Bz_NGP/conf_07 (**IB**)	O,3B	1.50	0.62	0.12
C2_Bz_NGP/conf_08	3S1	1.51	7.85	7.39
C2_Bz_NGP/conf_09	3S1	1.52	8.18	7.24
C4_Fmoc_RP/conf_00 (**II**)	5S1	3.09	56.36	56.28
C4_Fmoc_RP/conf_01	5S1	3.73	66.10	67.72
C4_Fmoc_RP/conf_02	3S1	2.88	87.33	83.42
C4_Fmoc_RP/conf_03	3S1	4.10	71.92	70.57
C4_Fmoc_RP/conf_04	3S1	2.96	66.65	65.53
oxocarbenium/conf_00 (**IV**)	E4	3.61	87.66	83.94
oxocarbenium/conf_01	2H3	3.74	91.25	88.21
oxocarbenium/conf_02	5H4	3.56	86.24	84.68
oxocarbenium/conf_03	E4	3.61	93.06	88.60
oxocarbenium/conf_04	5H4	3.58	131.71	124.56

Table S6. List of reoptimized geometries of the **Glc2** glycosyl cation at the PBE0+D3/6-311+G(d,p) level of theory. Ring puckers, bond distances between the carbonyl oxygen of the C2-benzoyl group and the anomeric carbon (C1), energies (Δ*E*, including zero-point-vibrational energy) and free energies (Δ*F*) at 90 K are assigned to each structure. The infrared spectra of the structures labelled with a roman number are represented in the manuscript.

ID	Ring Pucker	d(C2=O—C1) [Å]	Δ*E*(PBE0+D3) [kJ mol^{-1}]	Δ*F*(PBE0+D3) [kJ mol^{-1}]
C2_Bz_NGP/conf_00 (**IA**)	3S1	1.51	0.00	0.00
C2_Bz_NGP/conf_01	3S1	1.52	24.18	21.56
C2_Bz_NGP/conf_02	3S1	1.52	14.29	12.90
C2_Bz_NGP/conf_03 (**IB**)	3S1	1.51	4.53	4.89
C2_Bz_NGP/conf_04	3S1	1.52	24.30	22.00
C2_Bz_NGP/conf_05	3S1	1.52	25.66	23.12
C2_Bz_NGP/conf_06	OS2	1.52	8.12	8.44
C2_Bz_NGP/conf_07	3S1	1.51	12.66	11.52
C2_Bz_NGP/conf_08	3S1	1.51	19.76	19.10
C2_Bz_NGP/conf_09	O,3B	1.52	23.49	22.32
C6_Fmoc_RP/conf_00	5HO	3.02	96.30	95.54
C6_Fmoc_RP/conf_01	2SO	3.72	105.14	103.81
C6_Fmoc_RP/conf_02 (**II**)	2SO	3.15	95.80	94.88
oxocarbenium/conf_00	E4	2.93	104.93	98.63
oxocarbenium/conf_01	5H4	3.65	86.22	83.25
oxocarbenium/conf_02 (**IV**)	3H4	3.96	84.98	82.85
oxocarbenium/conf_03	E4	3.71	99.05	95.39
oxocarbenium/conf_04	E3	3.70	130.36	122.22

Table S7. List of reoptimized geometries of the **3F-Glc2** glycosyl cation at the PBE0+D3/6-311+G(d,p) level of theory. Ring puckers, bond distances between the carbonyl oxygen of the C2-benzoyl group and the anomeric carbon (C1), energies (Δ*E*, including zero-point-vibrational energy) and free energies (Δ*F*) at 90 K are assigned to each structure. The infrared spectra of the structures labelled with a roman number are represented in the manuscript.

ID	Ring Pucker	d(C2=O—C1) [Å]	Δ*E*(PBE0+D3) [kJ mol^{-1}]	Δ*F*(PBE0+D3) [kJ mol^{-1}]
C2_Bz_NGP/conf_00	3S1	1.51	10.93	10.27
C2_Bz_NGP/conf_01	4H5	1.54	10.90	10.75
C2_Bz_NGP/conf_02 (**IA**)	5H4	1.53	0.00	0.00
C2_Bz_NGP/conf_03	3S1	1.52	11.98	11.68
C2_Bz_NGP/conf_04	3S1	1.52	16.49	17.07
C2_Bz_NGP/conf_05	3S1	1.51	7.92	8.76
C2_Bz_NGP/conf_06	5H4	1.52	6.39	4.72
C2_Bz_NGP/conf_07	OS2	1.49	7.14	6.75
C2_Bz_NGP/conf_08	5H4	1.53	0.01	0.00
C2_Bz_NGP/conf_09 (**IB**)	OS2	1.50	3.64	3.22
C6_Fmoc_RP/conf_00 (**II**)	1C4	3.05	66.09	65.66
C6_Fmoc_RP/conf_01	1C4	3.02	77.83	77.11
C6_Fmoc_RP/conf_02	2SO	3.35	75.75	74.67
C6_Fmoc_RP/conf_03	2SO	3.52	93.28	91.74
C6_Fmoc_RP/conf_04	BO,3	3.37	98.23	95.88
oxocarbenium/conf_00 (**IV**)	5H4	3.73	65.81	64.03
oxocarbenium/conf_01	5H4	3.81	67.48	65.86
oxocarbenium/conf_02	4H3	3.64	98.81	95.56
oxocarbenium/conf_03[(a)]	5HO	4.01	67.64	67.64
oxocarbenium/conf_04	E4	3.59	97.75	93.99

(a) The structure "oxocarbenium/conf_03" converged into a dioxolenium-type structure exhibiting remote participation of the C6-Fmoc protecting group after reoptimization of the geometry at the PBE0+D3/6-311+G(d,p) level of theory and was therefore not further considered.

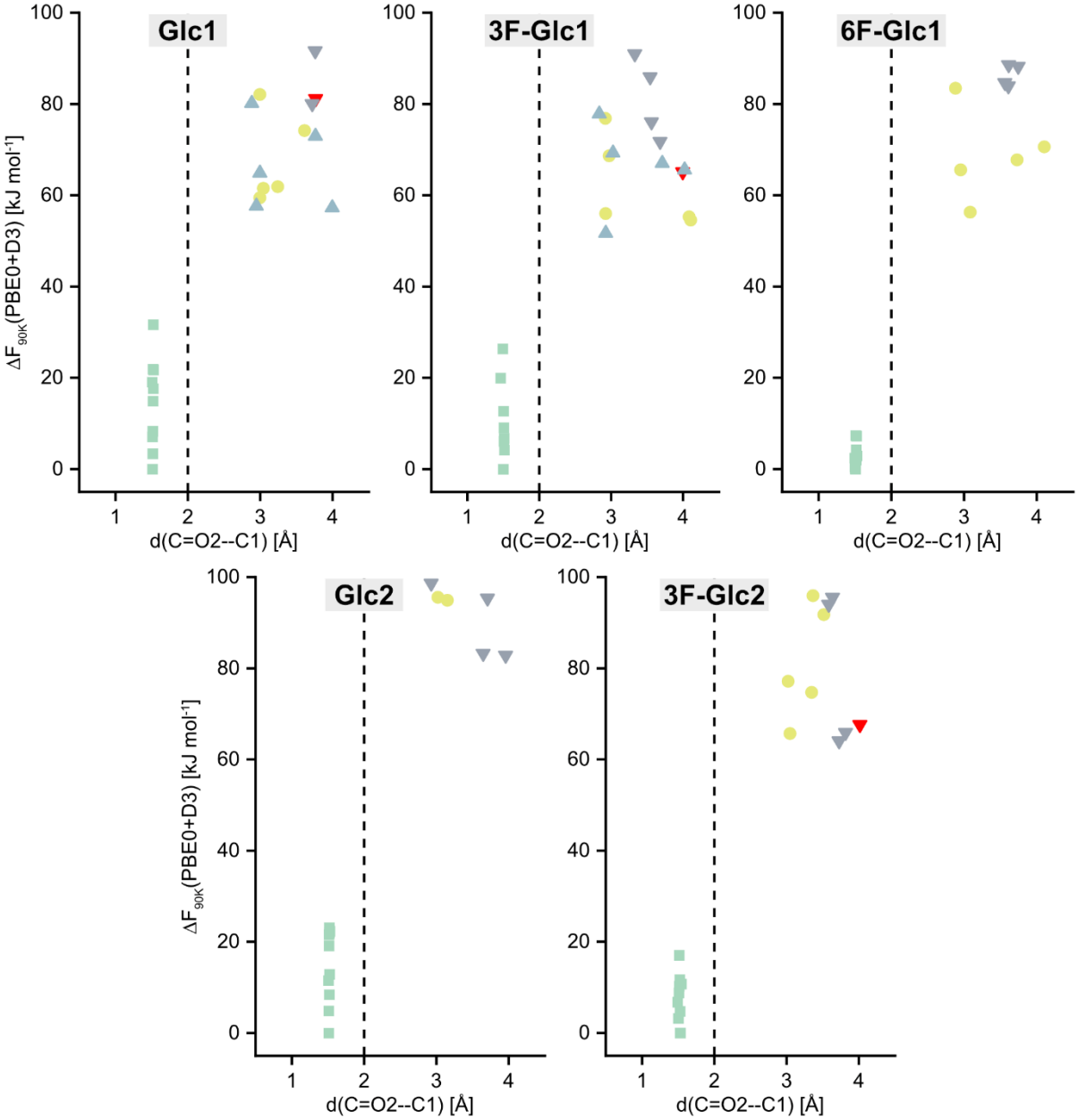

Figure S8. Energy hierarchies of reoptimized **Glc1**, **3F-Glc1**, **6F-Glc1**, **Glc2**, and **3F-Glc2** glycosyl cations as a function of the distance between the carbonyl oxygen of the C2-benzoyl protecting group and the anomeric carbon (C1). Free energies at 90 K were computed based on optimized geometries at the PBE0+D3/6-311+G(d,p) level of theory. Green squares indicate structures exhibiting C2-benzoyl neighboring group participation (**I**, dioxolenium), yellow circles C4-Fmoc remote participation (**II**, dioxolenium), blue triangles *non-classical* C6-benzyl remote participation (**III**, oxonium), and gray triangles no participation (**IV**, oxocarbenium). Red triangles represent former oxocarbenium-type structures that converged into another structural motif during reoptimization of the geometry. As they were not the lowest-energy structure of that motif, they were not further considered.

Low-Energy Structures

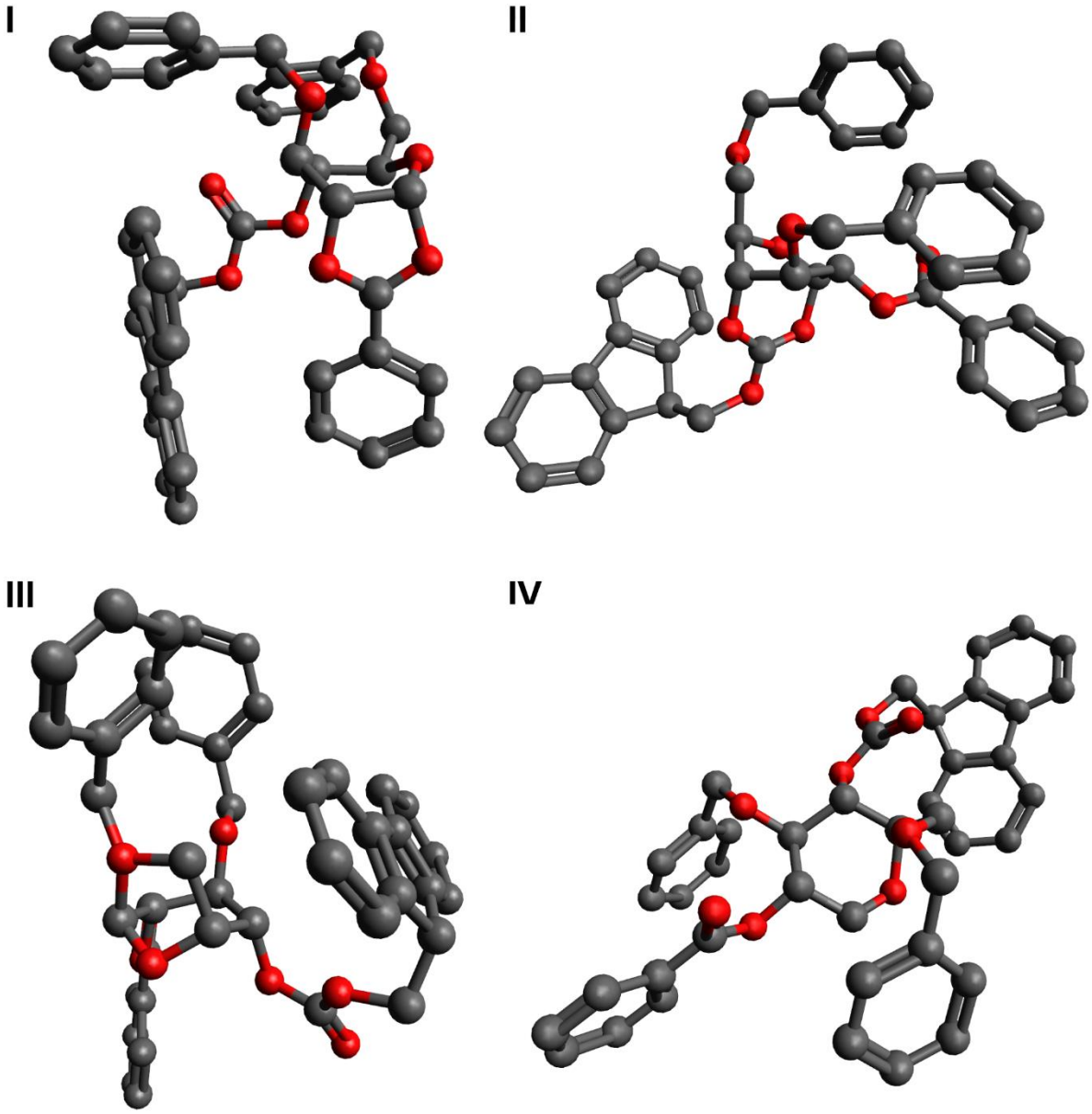

Figure S9. Reoptimized geometries of **Glc1** glycosyl cations exhibiting (**I**) C2-benzoyl neighboring group participation (C2_Bz_NGP/conf_00), (**II**) C4-Fmoc remote participation (C4_Fmoc_RP/conf_03), (**III**) C6-OBn *non-classical* remote participation (C6_OBn_RP/conf_01), and (**IV**) no participation (oxocarbenium/conf_00). Hydrogens are omitted for clarity.

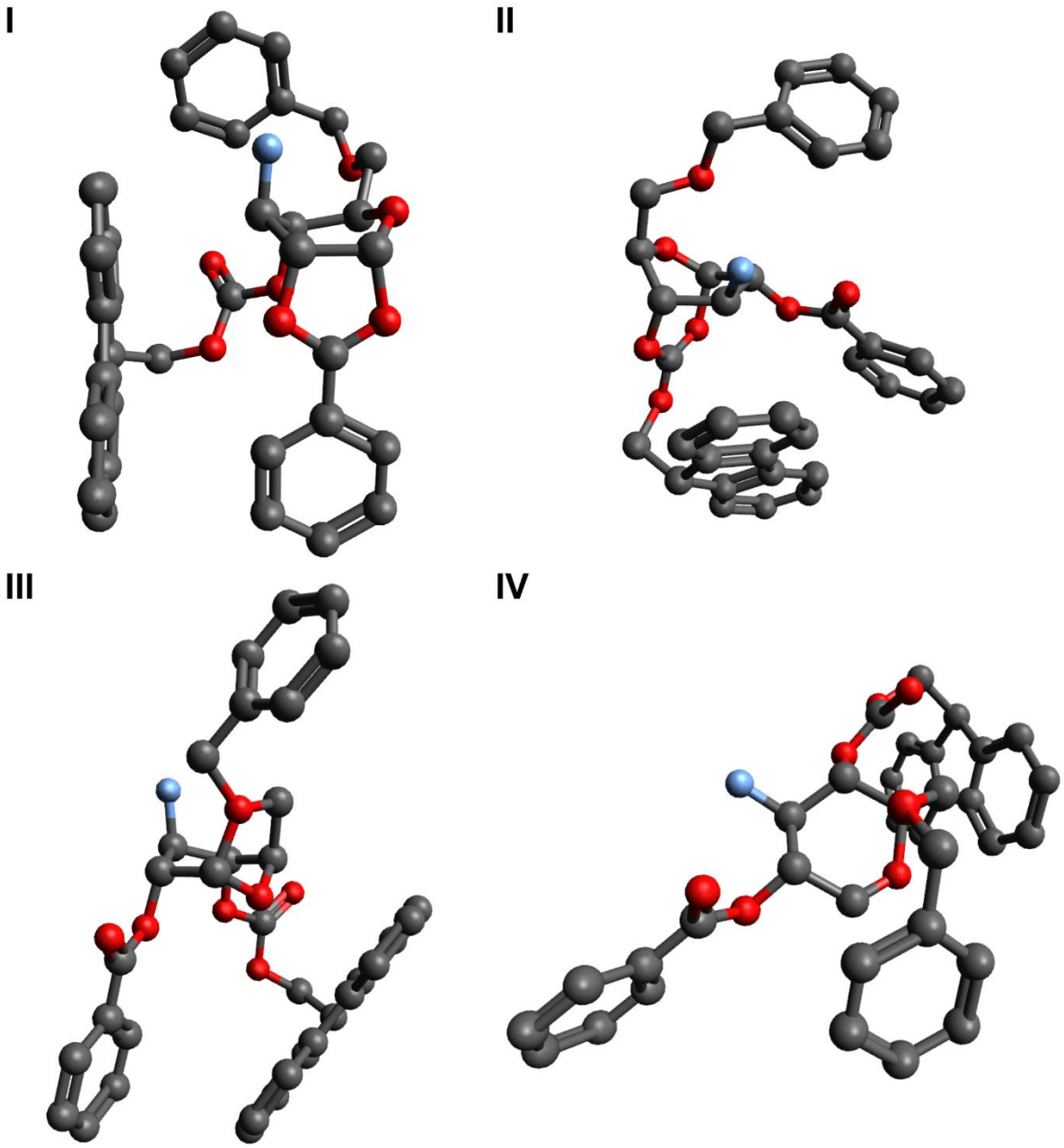

Figure S10. Reoptimized geometries of **3F-Glc1** glycosyl cations exhibiting (**I**) C2-benzoyl neighboring group participation (C2_Bz_NGP/conf_00), (**II**) C4-Fmoc remote participation (C4_Fmoc_RP/conf_03), (**III**) C6-OBn *non-classical* remote participation (C6_OBn_RP/conf_00), and (**IV**) no participation (oxocarbenium/conf_00). Hydrogens are omitted for clarity.

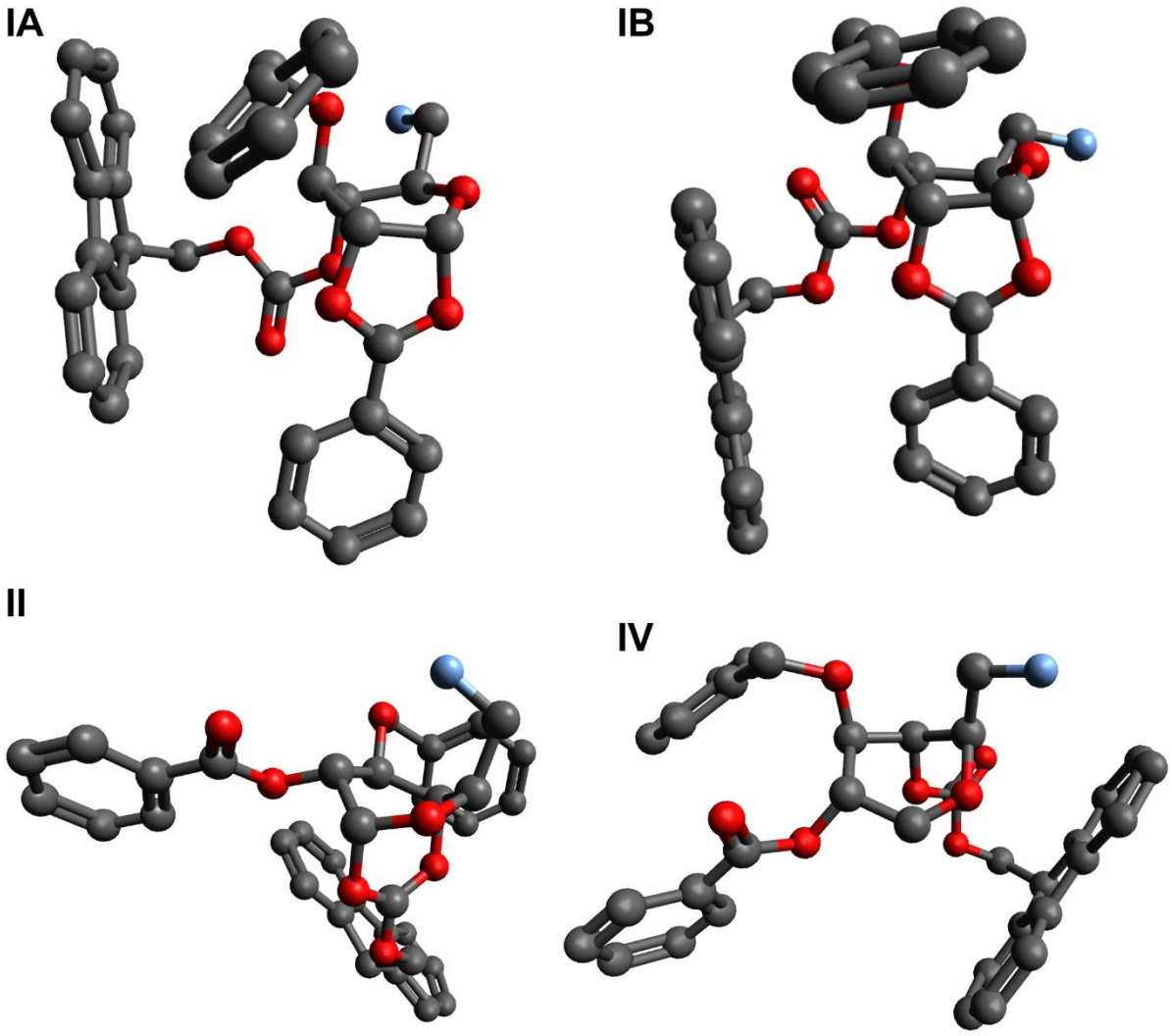

Figure S11. Reoptimized geometries of **6F-Glc1** glycosyl cations exhibiting (**I**) C2-benzoyl neighboring group participation (**A** C2_Bz_NGP/conf_01 and **B** C2_Bz_NGP/conf_07), (**II**) C4-Fmoc remote participation (C4_Fmoc_RP/conf_00), and (**IV**) no participation (oxocarbenium/conf_00). Hydrogens are omitted for clarity.

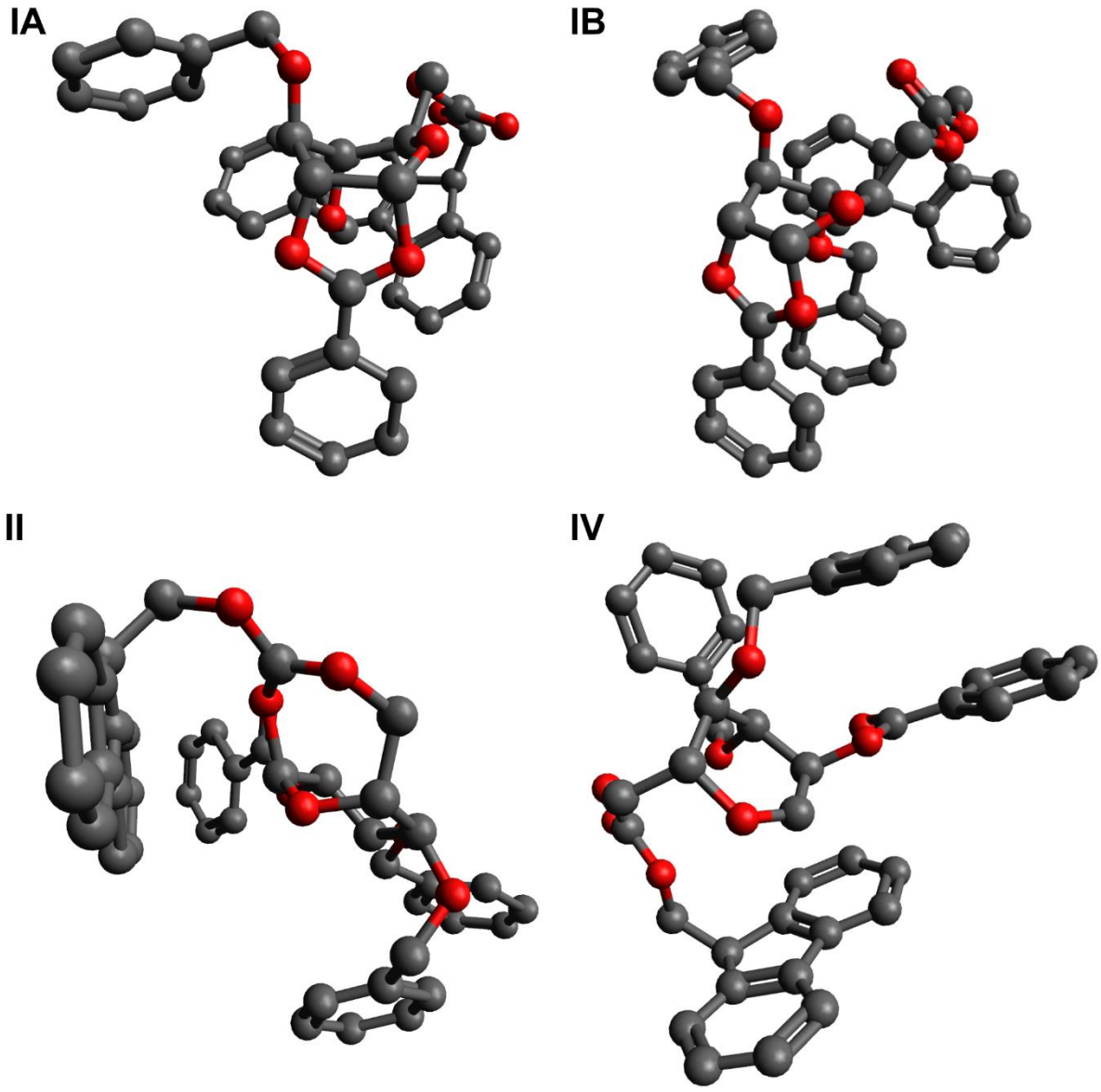

Figure S12. Reoptimized geometries of **Glc2** glycosyl cations exhibiting (**I**) C2-benzoyl neighboring group participation (**A** C2_Bz_NGP/conf_00 and **B** C2_Bz_NGP/conf_03), (**II**) C6-Fmoc remote participation (C4_Fmoc_RP/conf_02), and (**IV**) no participation (oxocarbenium/conf_02). Hydrogens are omitted for clarity.

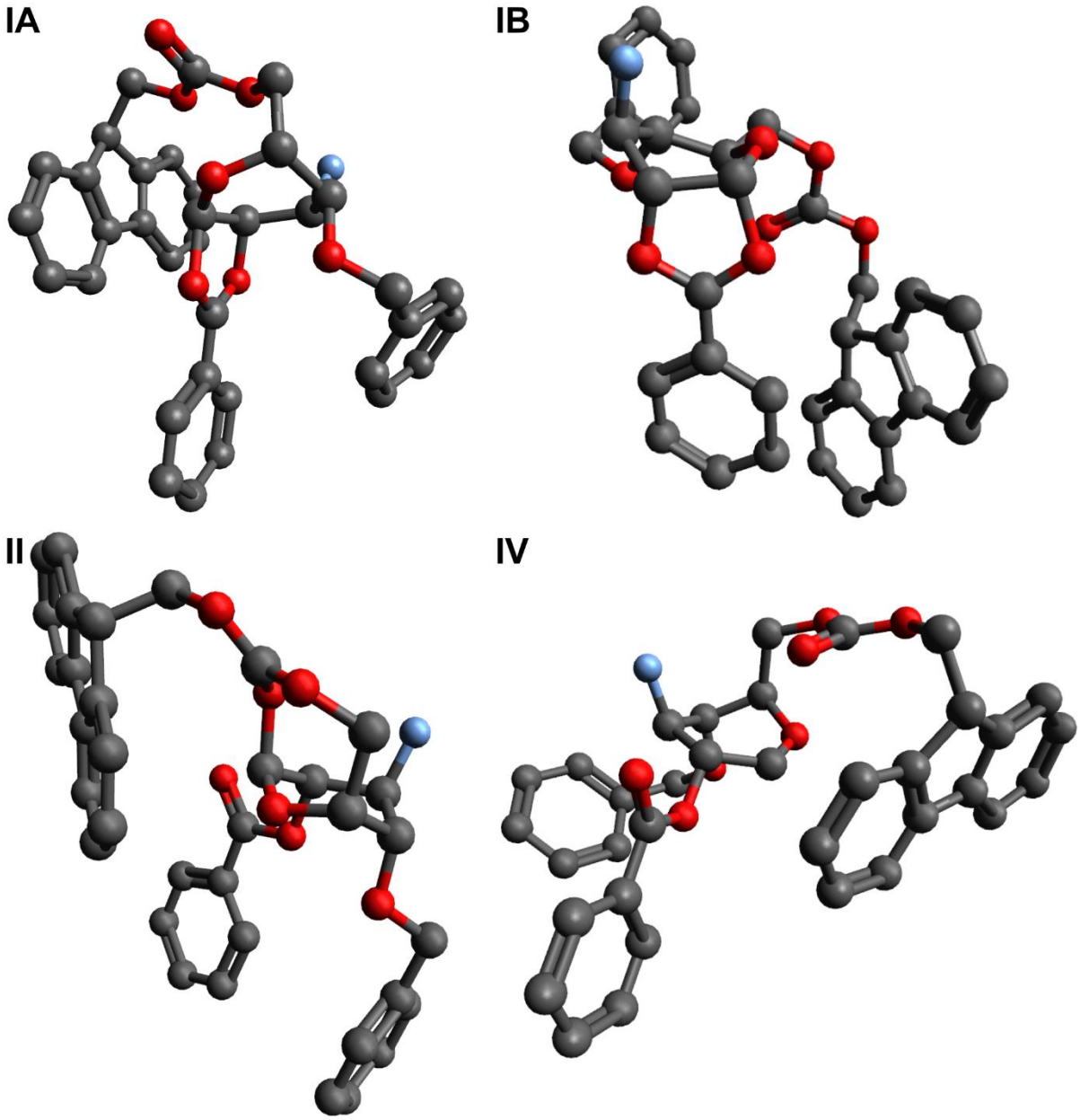

Figure S13. Reoptimized geometries of **3F-Glc2** glycosyl cations exhibiting (**I**) C2-benzoyl neighboring group participation (**A** C2_Bz_NGP/conf_02 and **B** C2_Bz_NGP/conf_09), (**II**) C6-Fmoc remote participation (C4_Fmoc_RP/conf_00), and (**IV**) no participation (oxocarbenium/conf_00). Hydrogens are omitted for clarity.

xyz-Coordinates of Reoptimized Structures

xyz-Coordinates of all reoptimized geometries can be found in a separate document "coordinates.xyz".

Synthesis of Building Blocks

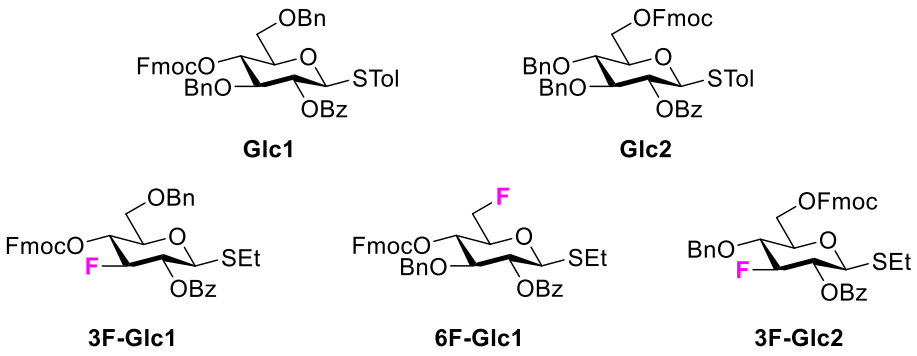

Scheme S1. Building blocks (BBs) used in this study.

Building blocks **Glc1** and **Glc2** were purchased from GlycoUniverse (Germany). **3F-Glc1** and **3F-Glc2** were synthesized as previously reported.[7] The synthesis of **6F-Glc1** is reported hereafter.

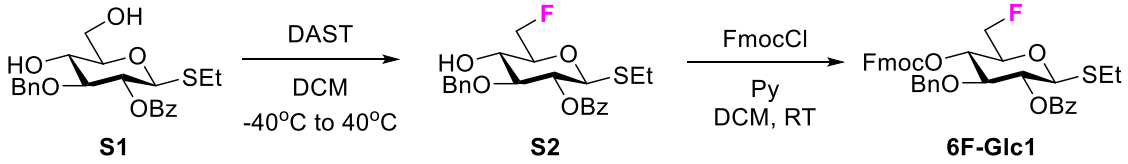

Scheme S2. Synthesis of fluorinated BBs **6F-Glc1**.

Synthesis of ethyl 2-*O*-benzoyl-3-*O*-benzyl-6-deoxy-6-fluoro-1-thio-β-D-glucopyranoside, S2

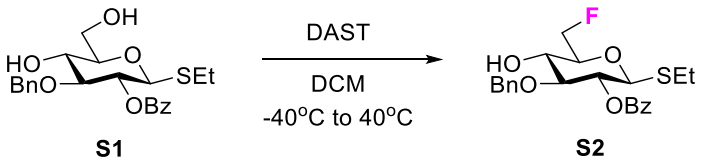

S1 was prepared according to previously established procedures.[8]

Ethyl 2-*O*-benzoyl-3-*O*-benzyl-6-1-thio-β-D-glucopyranoside **S1** (490 mg, 1.17 mmol) was dissolved in anhydrous DCM (10 mL) and cooled to -40°C (dry ice/ACN bath) under Ar atmosphere. DAST (171 µL, 1.29 mmol) was dissolved in anhydrous DCM (200 µL) and added dropwise to the reaction mixture. After 30 min the cooling bath was removed and the reaction heated up to 40 °C. The solution was stirred for additional 5 h and quenched with MeOH at 0 °C. The crude reaction mixture was diluted with DCM and washed once with brine. The crude

compound was purified by silica gel flash column chromatography (Hexane : EtOAc = 3:1→1:1) to give **S2** as a colorless oil (167 mg, 34%).

^{1}H NMR (400 MHz, Chloroform-*d*) δ 8.11 – 8.02 (m, 2H), 7.64 – 7.56 (m, 1H), 7.47 (tt, *J* = 6.7, 1.2 Hz, 2H), 7.32 – 7.15 (m, 5H), 5.36 – 5.24 (m, 1H), 4.81 – 4.51 (m, 5H), 3.78 – 3.67 (m, 2H), 3.58 (dddd, *J* = 21.5, 8.3, 5.0, 2.7 Hz, 1H), 2.82 – 2.63 (m, 2H), 2.34 (s, 1H), 1.24 (t, *J* = 7.5 Hz, 5H). ^{13}C NMR (101 MHz, Chloroform-*d*) δ 165.34, 137.77, 133.51, 129.99, 129.79, 128.78, 128.66, 128.29, 128.17, 84.14, 83.80, 82.19 (d, *J* = 173.4 Hz), 78.55 (d, *J* = 18.6 Hz), 74.94, 72.25, 69.07 (d, *J* = 7.2 Hz), 24.12, 14.92. ^{19}F NMR (376 MHz, Chloroform-*d*) δ -233.66 (td, *J* = 47.3, 22.8 Hz). $[\alpha]_D^{20}$ -18.12 (c 1.2 g/100 mL, $CHCl_3$). IR ν = 3482, 2927, 1724, 1268, 1086, 1070, 1027, 710, 700 cm^{-1}. (ESI-HRMS) m/z 443.1291 $[M+Na]^+$ ($C_{22}H_{25}FO_5SNa$ requires 443.1302).

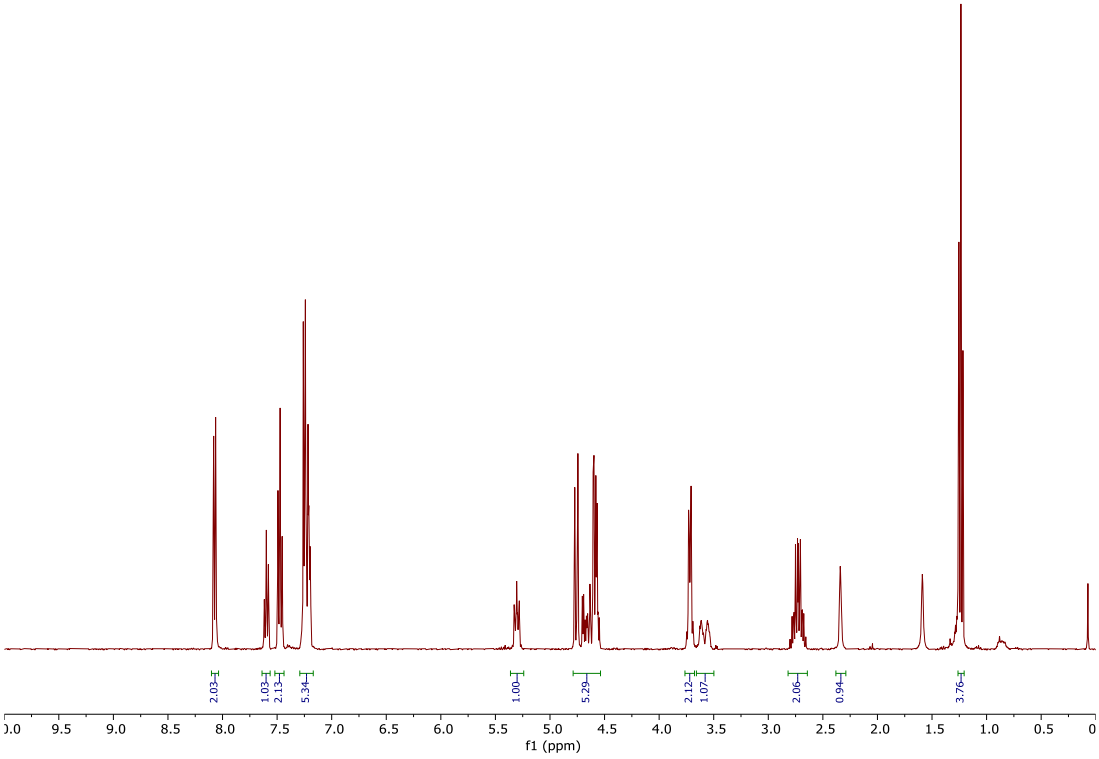

Figure S14. ^{1}H-NMR spectrum of **S2** (400 MHz, Chloroform-*d*).

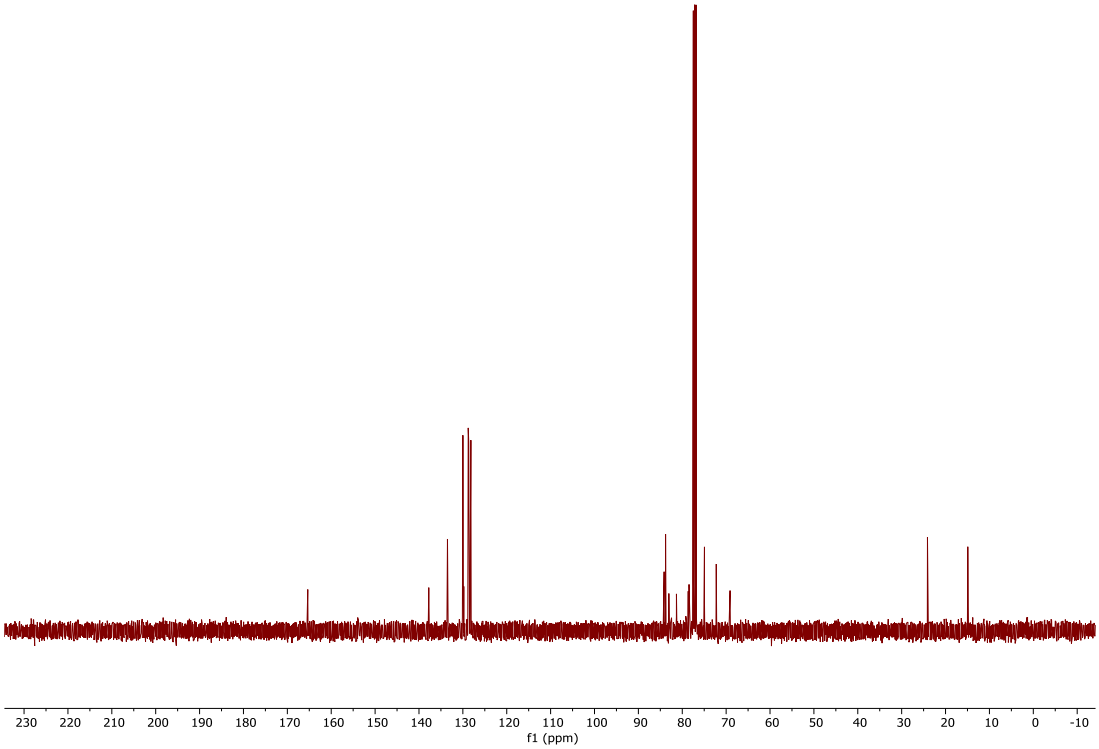

Figure S15. ^{13}C-NMR spectrum of **S2** (101 MHz, Chloroform-*d*).

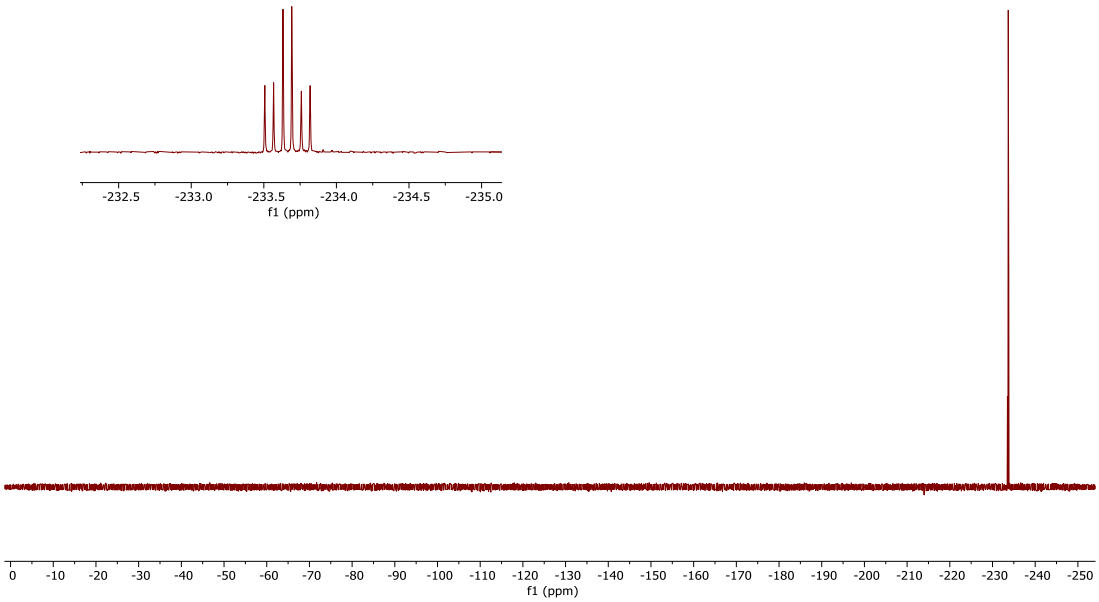

Figure S16. ^{19}F-NMR spectrum of **S2** (376 MHz, Chloroform-*d*).

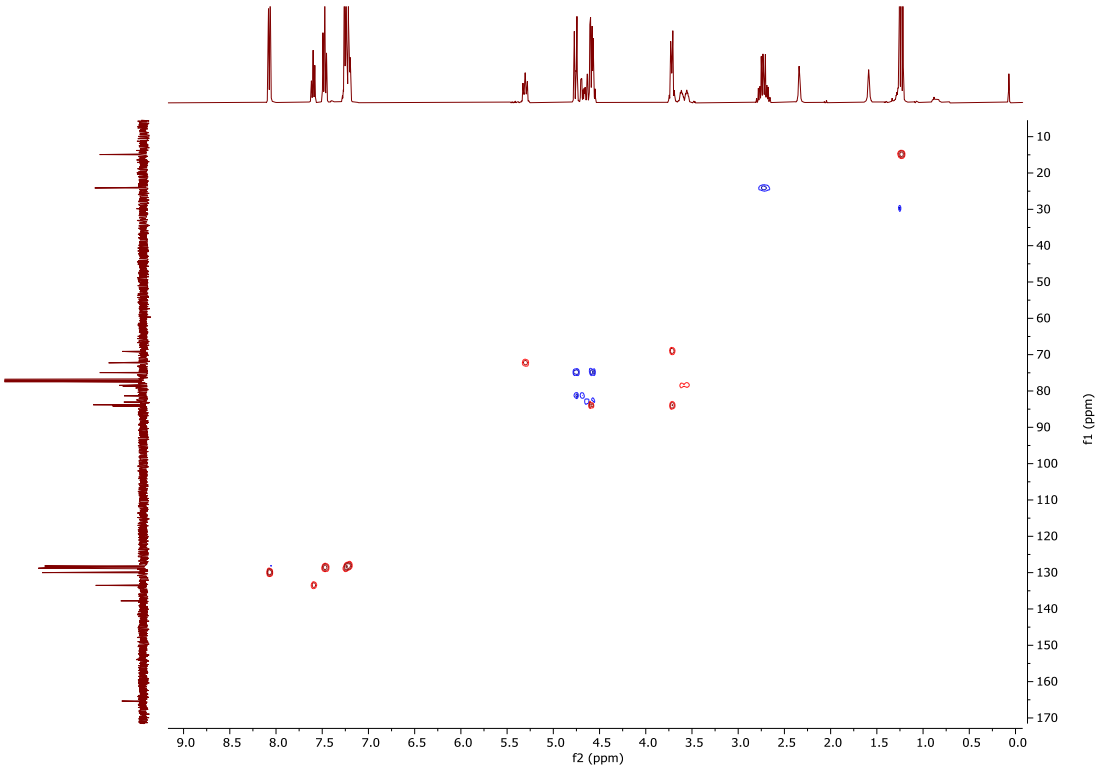

Figure S17. HSQC-NMR spectrum of **S2** (Chloroform-*d*).

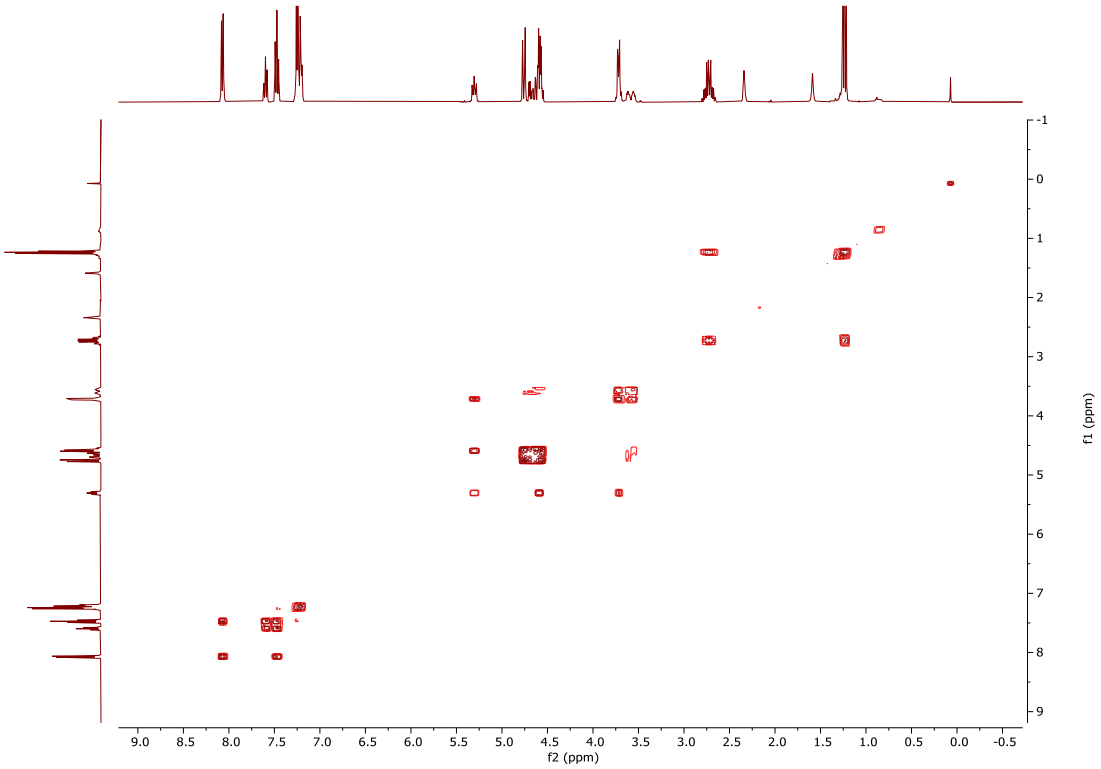

Figure S18. COSY-NMR spectrum of **S2** (Chloroform-*d*).

Synthesis of ethyl 2-*O*-benzoyl-3-*O*-benzyl-4-*O*-(9-fluorenylmethoxycarbonyl)-6-deoxy-6-fluoro-1-thio-β-D-glucopyranoside, 6F-Glc1

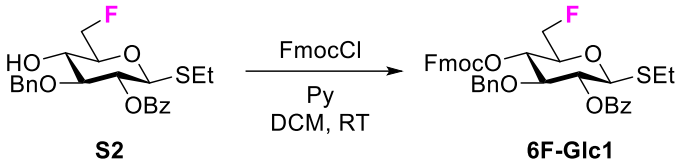

S2 **6F-Glc1**

Ethyl 2-*O*-benzoyl-3-*O*-benzyl-6-deoxy-6-fluoro-1-thio-β-D-glucopyranoside **S2** (167 mg, 0.40 mmol) was dissolved in DCM (5 mL) and pyridine was added (100 µL, 1.2 mmol). FmocCl (200 mg, 0.77 mmol) was dissolved in DCM (1.5 mL) and added to the reaction mixture at RT under Ar atmosphere. The solution was stirred for 3 h and then quenched with a 1 M solution of HCl. The crude reaction mixture was diluted with DCM, washed once with 1 M HCl, and once with brine. The crude compound was purified by silica gel flash column chromatography (Toluene : DCM = 4:1→3:1 then Toluene : EtOAc = 4:1) and precipitated from DCM : Hexane to give the **6F-Glc1** as a white solid (186 mg, 72%).

^{1}H NMR (400 MHz, Chloroform-*d*) δ 8.05 – 7.96 (m, 2H), 7.81 – 7.72 (m, 2H), 7.66 – 7.53 (m, 3H), 7.50 – 7.36 (m, 4H), 7.30 (tt, J = 7.5, 1.0 Hz, 2H), 7.20 – 7.00 (m, 5H), 5.33 (dd, J = 10.0, 9.1 Hz, 1H), 4.95 (dd, J = 10.2, 9.2 Hz, 1H), 4.63 – 4.49 (m, 5H), 4.48 – 4.40 (m, 2H), 4.20 (t, J = 6.8 Hz, 1H), 3.91 (t, J = 9.1 Hz, 1H), 3.82 – 3.69 (m, 1H), 2.82 – 2.65 (m, 2H), 1.23 (t, J = 7.5 Hz, 3H). ^{13}C NMR (101 MHz, Chloroform-*d*) δ 164.99, 154.17, 143.08, 143.04, 141.36, 137.18, 133.38, 129.91, 129.54, 128.48, 128.21, 128.00, 127.88, 127.73, 127.24, 125.04, 124.91, 120.17, 120.15, 83.69, 81.56 (d, J = 175.3 Hz), 80.81, 76.73, 74.45, 73.92 (d, J = 6.2 Hz), 71.64, 70.14, 46.79, 24.00, 14.80. ^{19}F NMR (376 MHz, Chloroform-*d*) δ -230.76 (td, J = 47.0, 20.0 Hz). $[\alpha]_D^{20}$ 23.35 (c 0.6 g/100 mL, $CHCl_3$). IR ν = 2928, 1754, 1729, 1248, 1028, 742, 710 cm^{-1}. (ESI-HRMS) m/z 665.1992 $[M+Na]^+$ ($C_{37}H_{35}FO_7SNa$ requires 665.1980).

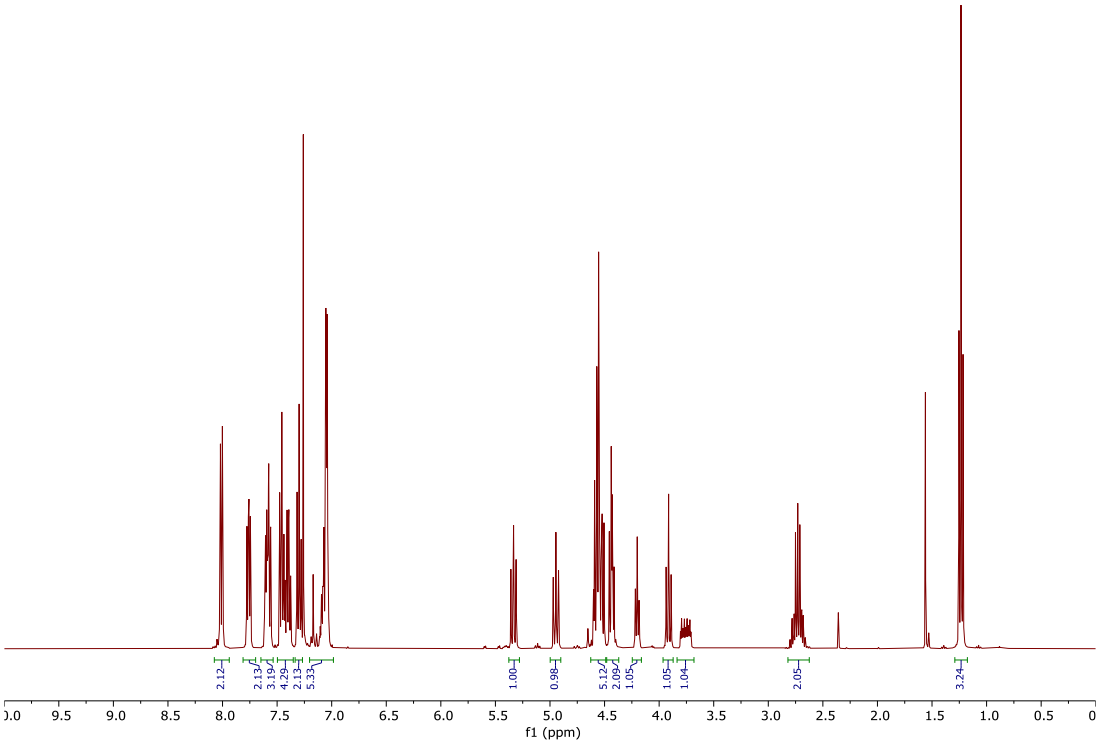

Figure S19. ^{1}H-NMR spectrum of **6F-Glc1** (400 MHz, Chloroform-*d*).

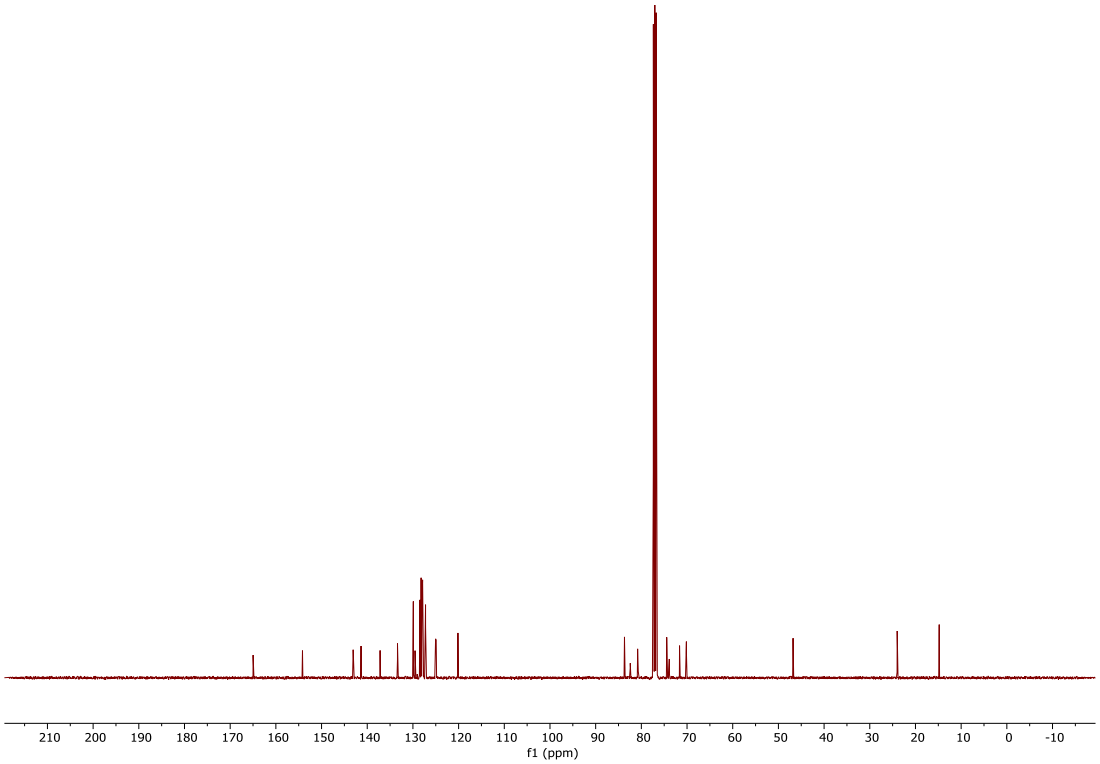

Figure S20. ^{13}C-NMR spectrum of **6F-Glc1** (101 MHz, Chloroform-*d*).

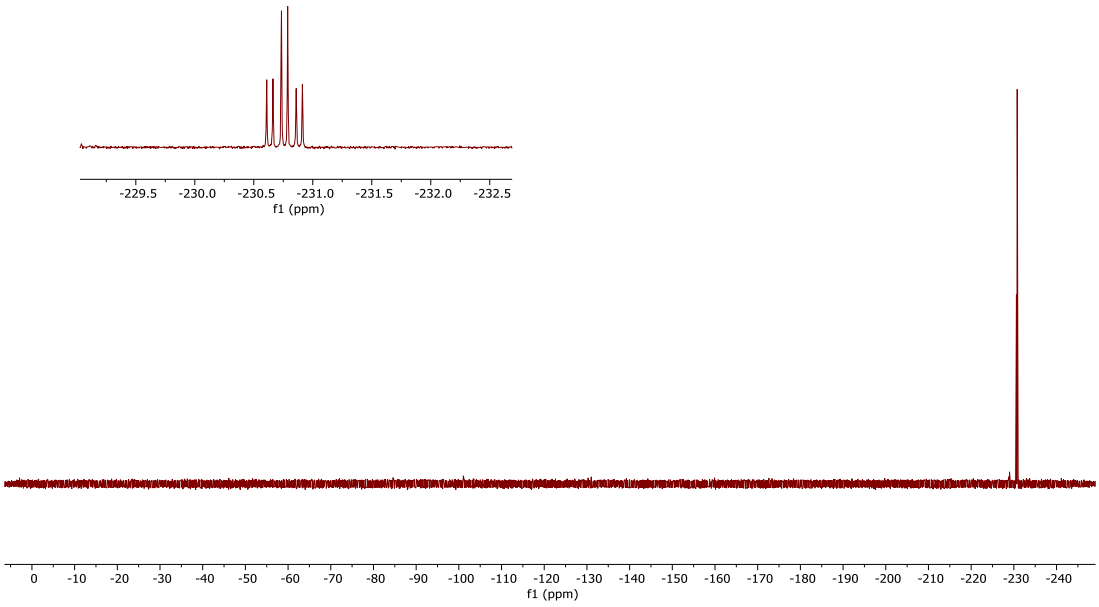

Figure S21. ^{19}F-NMR spectrum of **6F-Glc1** (376 MHz, Chloroform-*d*).

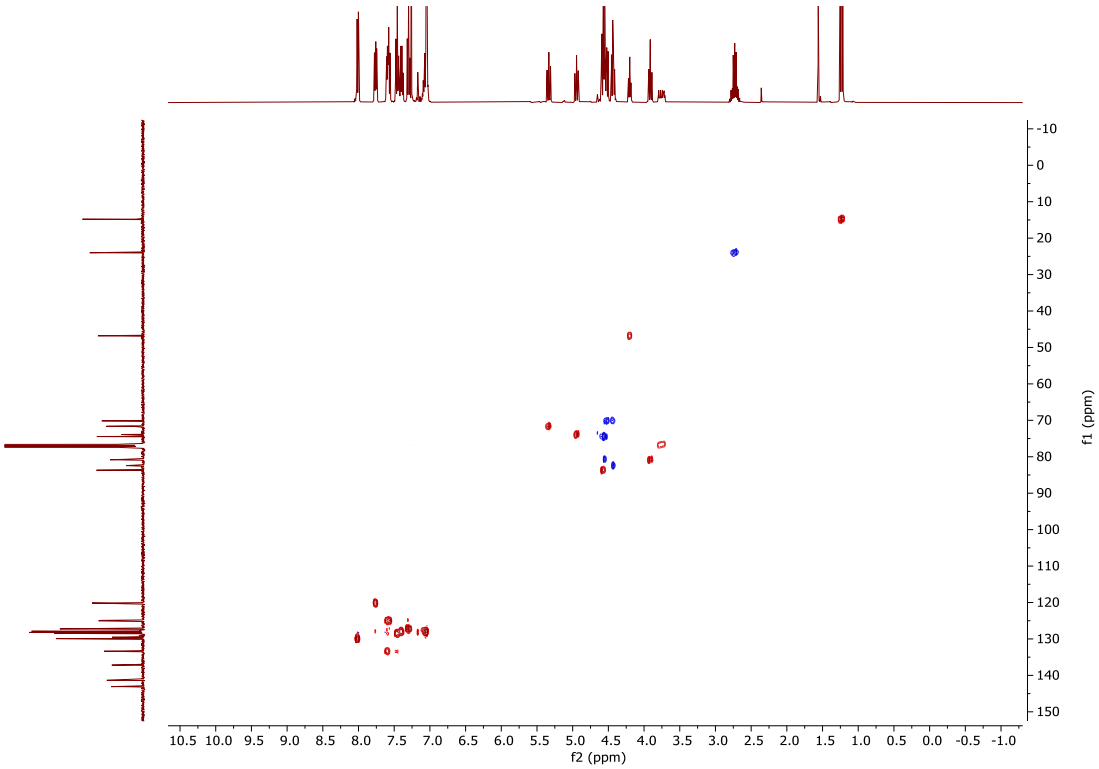

Figure S22. HSQC-NMR spectrum of **6F-Glc1** (Chloroform-*d*).

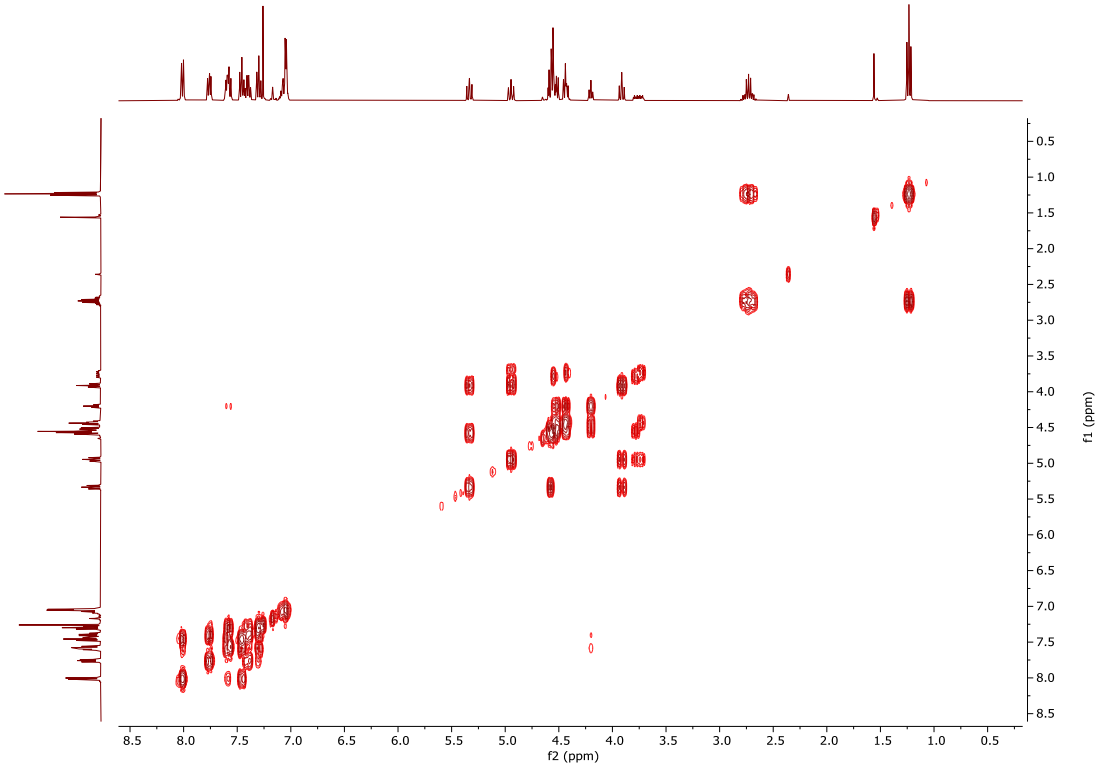

Figure 23. COSY-NMR spectrum of **6F-Glc1** (Chloroform-*d*).

References

[1] W. Schöllkopf, S. Gewinner, H. Junkes, A. Paarmann, G. von Helden, H. P. Bluem, A. M. M. Todd, *Proc. SPIE Int. Soc. Opt. Eng.* **2015**, *9512*, 95121L.

[2] A. Supady, V. Blum, C. Baldauf, *J. Chem. Inf. Model.* **2015**, *55*, 2338.

[3] F. Neese, *WIREs Comput. Mol. Sci.* **2012**, *2*, 73.

[4] a) J. P. Perdew, K. Burke, M. Ernzerhof, *Phys. Rev. Lett.* **1996**, *77*, 3865; b) F. Weigend, R. Ahlrichs, *Phys. Chem. Chem. Phys.* **2005**, *7*, 3297.

[5] a) C. Adamo, V. Barone, *J. Chem. Phys.* **1999**, *110*, 6158; b) S. Grimme, J. Antony, S. Ehrlich, H. Krieg, *J. Chem. Phys.* **2010**, *132*, 154104.

[6] M. J. Frisch, G. W. Trucks, H. B. Schlegel, G. E. Scuseria, M. A. Robb, J. R. Cheeseman, G. Scalmani, V. Barone, G. A. Petersson, H. Nakatsuji, X. Li, M. Caricato, A. V. Marenich, J. Bloino, B. G. Janesko, R. Gomperts, B. Mennucci, H. P. Hratchian, J. V. Ortiz, A. F. Izmaylov, J. L. Sonnenberg, Williams, F. Ding, F. Lipparini, F. Egidi, J. Goings, B. Peng, A. Petrone, T. Henderson, D. Ranasinghe, V. G. Zakrzewski, J. Gao, N. Rega, G. Zheng, W. Liang, M. Hada, M. Ehara, K. Toyota, R. Fukuda, J. Hasegawa, M. Ishida, T. Nakajima, Y. Honda, O. Kitao, H. Nakai, T. Vreven, K. Throssell, J. A. Montgomery Jr., J. E. Peralta, F. Ogliaro, M. J. Bearpark, J. J. Heyd, E. N. Brothers, K. N. Kudin, V. N. Staroverov, T. A. Keith, R. Kobayashi, J. Normand, K. Raghavachari, A. P. Rendell, J. C. Burant, S. S. Iyengar, J. Tomasi, M. Cossi, J. M. Millam, M. Klene, C. Adamo, R. Cammi, J. W. Ochterski, R. L. Martin, K. Morokuma, O. Farkas, J. B. Foresman, D. J. Fox, Wallingford, CT, **2016**.

[7] a) Y. Yu, T. Tyrikos-Ergas, Y. Zhu, G. Fittolani, V. Bordoni, A. Singhal, R. J. Fair, A. Grafmuller, P. H. Seeberger, M. Delbianco, *Angew. Chem. Int. Ed.* **2019**, *58*, 13127; b) S. Gim, G. Fittolani, Y. Yu, Y. Zhu, P. H. Seeberger, Y. Ogawa, M. Delbianco, *Chem. Eur. J.* **2021**, *27*, 13139.

[8] K. Zegelaar-Jaarsveld, S. A. W. Smits, G. A. van der Marel, J. H. van Boom, *Bioorg. Med. Chem.* **1996**, *4*, 1819.